Received: 14 February 2018 | Revised: 19 July 2018 | Accepted: 22 July 2018

DOI: 10.1002/aoc.4557

FULL PAPER

WILEY Applied Organometallic Chemistry

Mononuclear Co(III), Ni(II) and Cu(II) complexes of 2-(2,4-dichlorobenzamido)-*N′*-(3,5-di-*tert*-butyl-2-hydroxybenzylidene)benzohydrazide: Structural insight and biological assay

Geeta H. Chimmalagi[1] | Umashri Kendur[1] | Sunil M. Patil[1] | Christopher S. Frampton[2] | Kalagouda B. Gudasi[1] | Delicia A. Barretto[3] | Chandrashekhar V. Mangannavar[4] | Iranna S. Muchchandi[4]

[1] Department of Chemistry, Karnatak University, Dharwad 580003Karnataka, India

[2] Institute of Materials & Manufacturing, Wolfson Centre for Materials Processing, Brunel University, London, Uxbridge, UK

[3] Department of Biotechnology and Microbiology, Karnatak University, Dharwad 580003Karnataka, India

[4] H. S. K. College of Pharmacy, Bagalkot 587101Karnataka, India

Correspondence
Kalagouda B. Gudasi, Department of Chemistry, Karnatak University, Dharwad 580003, Karnataka, India.
Email: kbgudasi@gmail.com

A series of mononuclear metal complexes of Co(III), Ni(II) and Cu(II) with 2-(2,4-dichlorobenzamido)-*N′*-(3,5-di-*tert*-butyl-2-hydroxybenzylidene)benzohydrazide (**LH$_3$**) have been synthesized and characterized using various physico-chemical, spectroscopic and single crystal X-ray diffraction techniques. Structural studies of [Co(**LH**)(**LH$_2$**)]·H_2O (**4**) revealed the presence of both amido and imidol tautomeric forms of **LH$_3$**, resulting in a distorted octahedral geometry around the Co(III) ion. [Ni(**LH**)(H_2O)]·H_2O (**5**) and [Cu(**LH**)(H_2O)]·H_2O (**6**) are isomorphous structures and crystallize in the monoclinic $P2_1/c$ space group. The crystal structures of **4**, **5** and **6** are stabilized by hydrogen bonds formed by the enclathrated water molecules, C-H···π and π···π interactions. Complexes along with the ligand (**LH$_3$**) were screened for their *in vivo* anti-inflammatory activity (carrageenan-induced rat paw edema method) and *in vitro* antioxidant activity (DPPH free radical scavenging assay). Metal complexes have shown significant anti-inflammatory and antioxidant potential.

KEYWORDS
anti-inflammatory activity, antioxidant activity, crystal structure, di-*tert*-butyl phenylhydrazone, isomorphous metal complexes

1 | INTRODUCTION

Oxidation processes are requisite for life; however, they can have toxic potential effects as they generate excess free radicals that can cause oxidative damage to proteins, membranes and genes.[1–3] These reactive free radicals have been associated as mediators in an assortment of many diseases, such as arthritis, inflammation, cancer, neurological and heart diseases.[1,4–6] The reactive oxygen species generated by infiltrated neutrophils act as venomous agents that are involved in the cyclooxygenase-2 (COX-2) and 5-lipoxygenase (5-LOX) mediated conversion of arachidonic acid into proinflammatory intermediates, hence, enhancing the inflammatory process.[7–9] Therefore, the compounds with antioxidant/radical scavenging properties could be anticipated to offer protection in arthritis and inflammation. Many studies on commercially available nonsteroidal anti-inflammatory drugs

and their metal complexes have proven their simultaneous free radical scavenging properties.[10,11]

Aroylhydrazones (AHs) are an elite class of compounds that have drawn much attention as versatile ligands with a variety of coordination modes with transition metals.[12] AHs exhibit amido-imidol tautomerism in solution and coordinate to metal ions through its amido/imidol form. In exceptional cases, both forms simultaneously coordinate to the metal ion. The possibility of tautomerism in this class of compounds has proved attractive in the field of pharmacology. Most of the first row transition metals either alone or in their complex form are biologically important with a number of bioactivities. Transition metal complexes of AHs present a diverse range of biological applications, such as anti-inflammatory, antioxidant, antiproliferative and antitumor activities.[13–15] These transition metal complexes have shown greater biological potential than the proligands. In addition, transition metal complexes of AHs are known to act as efficient and selective catalysts towards various chemical reactions.[16,17]

Hydrazones containing di-*tert*-butyl phenol moiety as a key structural feature are of conspicuous interest, due to their diverse antioxidant, anticancer, antifungal, antibacterial and dual COX/LOX inhibitory activities.[18–20] An array of metal complexes of di-*tert*-butyl phenylhydrazones has been described in the literature.[16,17,21–24] Many of them did not divulge a biological relevance. Based on the above facts, our present endeavor emphasizes the synthesis, structural characterization, antioxidant and anti-inflammatory activities of transition metal complexes of newly synthesized tridentate di-*tert*-butyl phenylhydrazone (**LH_3**) derived from the condensation of 2-(2,4-dichlorobenzamido)benzohydrazide and 3,5-di-*tert*-butyl-2-hydroxybenzaldehyde.

2 | EXPERIMENTAL

2.1 | Materials and physical measurements

All the reagents and solvents were purchased commercially and used without further purification. Elemental analysis (C, H, N) was performed on Thermoquest CHN analyzer. The metal content of the complexes was determined according to the literature procedure.[25] ^{1}H and ^{13}C NMR spectra were measured on Bruker AV-400 and AGILENT VNMRS-400 spectrometer, respectively, in dimethylsulfoxide (DMSO)-d_6 with tetramethylsilane as an internal standard. Infrared (IR) spectra were recorded on a Nicolet-6700 FT-IR spectrometer using KBr discs in the 4000–400 cm^{-1} region. Absorbance spectra were recorded on a JASCO V-670 UV–Vis spectrophotometer. ESI-MS were recorded on a Waters XEVO TQS micromass spectrometer. EPR spectra were recorded at both room temperature and 77 K on a Varian E-4 X-band spectrometer. Conductance measurements of complexes (50 μM) were recorded in DMF using an ELICO-CM-82 conductivity bridge. Thermogravimetric analyses (TGA) were carried out over the temperature range of 25–1000°C using Universal V4.5A TA instrument.

2.2 | Synthesis of 2-(2,4-dichlorobenzamido)-*N′*-(3,5-di-*tert*-butyl-2-hydroxybenzylidene)benzohydrazide (LH_3)

LH_3 was prepared in three steps as reported earlier in a similar case.[26] In the first step, methyl anthranilate (**1**; 3.02 g, 20 mmol) was suspended in benzene (300 ml), to which 2,4-dichlorobenzoyl chloride (4.16 g, 20 mmol) was added and stirred for 3 h at room temperature to generate methyl 2-(2,4-dichlorobenzamido)benzoate (**2**; yield: 91%), which was then hydrazinolyzed at reflux temperature to produce 2-(2,4-dichlorobenzamido) benzohydrazide (**3**; yield: 76%). Finally, the methanolic solution of 3,5-di-*tert*-butyl-2-hydroxybenzaldehyde (2.34 g, 10 mmol) was added to a methanolic suspension of **3** (3.24 g, 10 mmol). The reaction mixture along with a catalytic amount of glacial acetic acid was refluxed for 3 h. Progress of the reaction was monitored by TLC. The white precipitate formed was filtered off, washed with hot methanol and dried in air. Schematic representation for the synthesis of **LH_3** is shown in Scheme 1.

LH_3: color: colorless. Isolated yield: 84%. m.p. 250–252°C. Anal. calcd for $C_{29}H_{31}Cl_2N_3O_3$: C, 64.44; H, 5.78; N, 7.77%. Found: C, 64.70; H, 5.53; N, 7.68%. IR (ν, KBr, cm^{-1}): 3444, 3326, 3232, 1680, 1660, 1607. ^{1}H-NMR (400 MHz, DMSO-d_6, δ, ppm): 1.28 (9H, s, *tert*-Bu), 1.39 (9H, s, *tert*-Bu), 7.20 (1H, d, C23H, J = 2 Hz), 7.31 (1H, d, C29H, J = 2 Hz), 7.34 (1H, t, C11H, J = 8 Hz), 7.65–7.58 (2H, m, C4H and C10H), 7.70 (1H, d, C5H, J = 8 Hz), 7.76 (1H, d, C2H, J = 1.6 Hz), 7.81 (1H, d, C9H, J = 7.6 Hz), 8.25 (1H, d, C12H, J = 8 Hz), 8.52 (1H, s, C15H), 11.13 (1H, s, O3H), 12.16 (1H, s, N2H), 12.33 (1H, s, N1H). ^{13}C-NMR (100 MHz, DMSO-d_6, δ, ppm): 29.77 ($(CH_3)_3$), 31.74 ($(CH_3)_3$), 34.34 (C-$(CH_3)_3$), 35.09 (C-$(CH_3)_3$), 117.35 (C16), 124.66 (C29), 126.28 (C23), 128.23 (C4), 130.10 (C5), 130.84 (C2), 131.73 (C6), 136.20, 122.73, 132.79, 126.28, 129.15, 123.16 (C8–13, aromatic), 135.24 (C1), 135.92 (C18), 138.12 (C3), 140.99 (C24), 152.37 (C15), 155.18 (C17), 164.19 (C14), 164.32 (C7). ESI-MS (m/z): 540 [**LH_3** + H]$^+$. UV–Vis: λ_{max}/nm (ε/dm^3 mol^{-1} cm^{-1}): 266 (38 846), 299 nm (55 756).

2.3 | Syntheses of metal complexes

2.3.1 | [Co(LH)(LH_2)]·H_2O (4)

A methanolic solution of $Co(CH_3COO)_2{\cdot}4H_2O$ (0.062 g, 0.25 mmol) was added dropwise to a methanolic suspension of **LH_3** (0.270 g, 0.5 mmol). The reaction mixture was then refluxed on a water bath for 4 h (Scheme 2a). The resultant solution was left to evaporate until reddish brown crystals of [Cu(LH)(H_2O)]H_2O suitable for X-ray diffraction studies were separated.

Color: reddish brown. Isolated yield: 76%. Anal. calcd for $C_{58}H_{61}Cl_4CoN_6O_7$: C, 60.32; H, 5.32; N, 7.28; Co, 5.10%. Found: C, 59.98; H, 5.14; N, 7.37; Co, 5.02%. IR (ν, KBr, cm^{-1}): 3423, 3347, 1681, 1612, 1585, 1320. ESI-MS (m/z): 1135 [Co(**LH**)(**LH_2**) + H]$^+$. UV–Vis: λ_{max}/nm (ε/dm^3 mol^{-1} cm^{-1}): 268 (79 700), 322 (30 915), 442 nm (21 348). Molar conductance (Ω^{-1} cm^2 mol^{-1}): 2.52.

2.3.2 | [Ni(LH)(H_2O)]·H_2O (5)

A mixture of **LH_3** (0.270 g, 0.5 mmol), sodium acetate (0.082 g, 2.0 mmol) and $NiCl_2{\cdot}6H_2O$ (0.119 g, 0.5 mmol) in methanol was refluxed on a water bath for 4 h (Scheme 2b), and the resultant solution was left to evaporate until reddish brown crystals of [Ni(**LH**)(H_2O)]·H_2O suitable for X-ray diffraction studies were separated.

Color: reddish brown. Isolated yield: 69%. Anal. calcd for $C_{29}H_{33}Cl_2N_3NiO_5$: C, 55.01; H, 5.25; N, 6.64; Ni, 9.27%. Found: C, 55.32; H, 5.17; Ni, 9.16; N, 6.52%. IR (ν, KBr, cm^{-1}): 3625, 3559, 3431, 1679, 1613, 1594, 1324. ^{1}H-NMR (400 MHz, $CDCl_3$, δ, ppm): 0.90 (9H, s, *tert*-Bu), 1.21 (9H, s, *tert*-Bu), 6.73–7.04 (4H, m, C23H, C29H, C10H and C11H), 7.27–7.47 (3H, m, C2H, C4H and C5H,) 8.19 (2H, d, C12H and C9H, J = 7.2 Hz), 8.69 (1H, s, C15H), 9.67 (1H, s, N1H). ^{13}C-NMR (100 MHz, $CDCl_3$, δ, ppm): 29.80 ($(CH_3)_3$), 30.79 ($(CH_3)_3$), 33.60 (C-$(CH_3)_3$), 35.25 (C-$(CH_3)_3$), 117.14 (C16), 121.23 (C29), 126.33 (C23), 127.84 (C4), 129.53 (C5), 130.79 (C2 and C6), 138.69, 120.13, 131.62, 124.12, 128.90, 136.53 (C8–13, aromatic), 132.25 (C1), 133.61 (C18), 137.75 (C3), 139.82 (C24), 153.12 (C17), 157.83 (C15), 162.06 (C7), 172.69 (C14). ESI-MS (m/z): 613 [Ni(**LH**)(NH_3) + H]$^+$. UV–Vis: λ_{max}/nm (ε/dm^3 mol^{-1} cm^{-1}): 267 (67 759), 320 (34 476), 428 nm (36 290). Molar conductance (Ω^{-1} cm^2 mol^{-1}): 4.91.

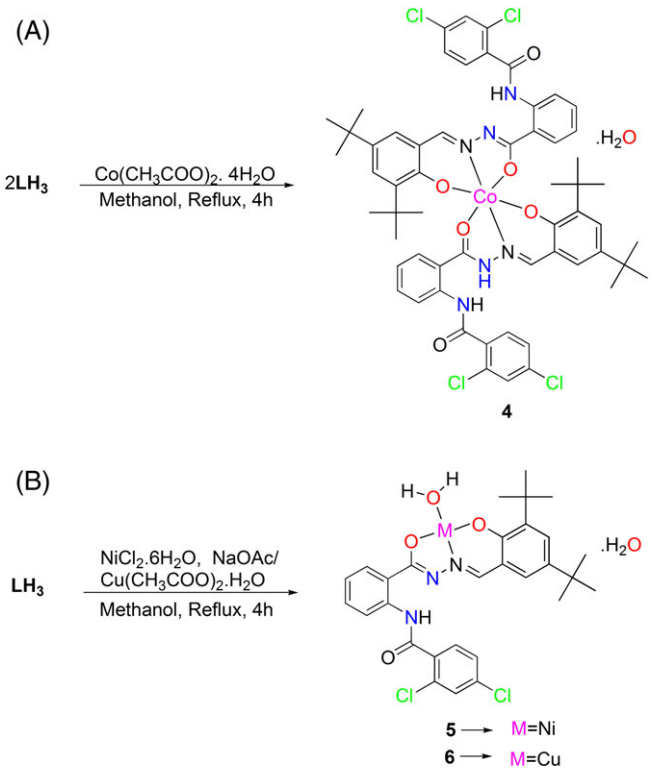

SCHEME 2 (a) Synthetic route for the preparation of [Co(**LH**)(**LH_2**)]·H_2O (**4**). (b) Synthetic route for the preparation of [Ni(**LH**)(**H_2O**)]·H_2O (**5**) and [Cu(**LH**)(**H_2O**)]·H_2O (**6**)

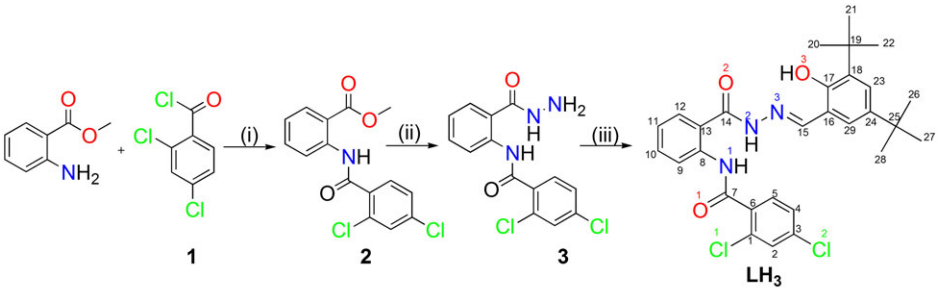

Reaction conditions: i) Benzene, R.T, 3 h. ii) $N_2H_4.H_2O$, MeOH, Reflux, 4 h. iii) 3,5-di-*tert*-butyl-2-hydroxybenzaldehye, MeOH, AcOH, Reflux, 3 h.

SCHEME 1 Synthetic route for the preparation of **LH_3**

2.3.3 | $[Cu(LH)(H_2O)]\cdot H_2O$ (6)

A methanolic solution of $Cu(CH_3COO)_2\cdot H_2O$ (0.10 g, 0.5 mmol) was added dropwise to a methanolic suspension of **LH_3** (0.270 g, 0.5 mmol). The reaction mixture was then refluxed on a water bath for 4 h (Scheme 2b). Single crystals of $[Cu(LH)(H_2O)]H_2O$ suitable for X-ray diffraction studies were obtained on slow evaporation of the resultant solution at ambient temperature.

Color: green. Isolated yield: 74%. Anal. calcd for $C_{29}H_{33}Cl_2CuN_3O_5$: C, 54.59; H, 5.21; Cu, 9.96; N, 6.59%. Found: C, 55.01; H, 5.23; Cu, 9.73; N, 6.45. IR (ν, KBr, cm^{-1}): 3644, 3553, 3442, 1677, 1611, 1589, 1318. ESI-MS (m/z): 618 $[Cu(\mathbf{LH})(NH_3) + H]^+$. UV–Vis: λ_{max}/nm (ε/dm^3 mol^{-1} cm^{-1}): 267 (67 493), 323 (40 145), 416 (37 988), 666 nm (612). Molar conductance (Ω^{-1} cm^2 mol^{-1}): 4.79.

2.4 | Single crystal X-ray diffraction studies

Single crystal data were collected at 100 K on a Rigaku SuperNova, Dualflex, AtlasS2 diffractometer using Cu-Kα radiation (λ = 1.54184 Å). CrysAlis Pro software was used for data collection, absorption correction and data reduction.[27] The structures were solved by a direct method with SHELXD-2014/6 and refined using SHELXL-2014/6 program package.[28] The structure of **4** was pseudo-centrosymmetric and could be solved in the space group *Pbca*; however, refinement in this setting has failed. As a consequence of the psuedosymmetry, the overall structure was refined as a two-component inversion twin with a final Flack parameter of 0.273(4). Hydrogen atom positions were calculated geometrically and refined using the riding model. Mercury CSD 2.0 program[29] was used for molecular graphics. The structural data have been deposited with the Cambridge Crystallographic Data Centre (CCDC) with reference numbers 1822746, 1822747 and 1822748 for **4**, **5** and **6**, respectively.

2.5 | DPPH radical scavenging activity

The antioxidant activity of the titled compounds was measured on the basis of the free radical scavenging activity by the 2,2-diphenyl-1-picrylhydrazyl (DPPH) method.[30] The stock solution of DPPH was prepared by dissolving 3.9432 mg DPPH in 100 ml of methanol (0.1 mM) and stored at 4°C until use; 2 ml of DPPH solution was mixed with 1 ml of different concentrations (20–100 $\mu g\ ml^{-1}$ in DMSO) of the compounds. The reaction mixture was mixed and incubated at room temperature in the dark for 30 min. The absorbance was recorded spectrophotometrically at 517 nm. A mixture of 1 ml distilled water and 2 ml DPPH solution was used as the control, and ascorbic acid as the standard. The experiment was performed in triplicate and the results were presented as means ± standard deviations (mean ± SD). The percent radical scavenging was calculated by the following equation

$$\text{DPPH scavenging effect}\% = [(A_c - A_t)/A_c] \times 100$$

where A_c is the absorbance of the control and A_t is the absorbance of the test compound. IC_{50} values were calculated from the plot of scavenging activity against the concentrations of the samples.

2.6 | Anti-inflammatory screening

The *in vivo* anti-inflammatory activity of the test compounds was performed by the carrageenan-induced rat paw edema method.[31] Male Sprague–Dawley rats weighing 160–220 g were divided into groups of six each. The experimental protocol was approved by Institutional Animal Ethics Committee (IAEC/2008/01–11/HSK), and the same procedure was carried at H. S. K. College of Pharmacy, Bagalkot. The hind paw edema was induced in each rat by the sub-plantar injection of 1% λ-carrageenan (0.2 ml in 0.9% NaCl) 1 h after the administration of the test compounds (5 and 10 mg kg^{-1} of body weight) and standard drug (Diclofenac, 10 mg kg^{-1} of body weight) orally. The control groups received 0.5% Na-CMC in distilled water. The volume of the paw was measured by means of a digital plethysmometer (UGO Basile 7140) at 0.5, 1, 3 and 5 h after injection of the inflammatory stimulus. The percent edema inhibition was calculated by the following equation

$$\%\text{edema inhibition} = [(V_c - V_t)/V_c] \times 100$$

where V_c is the edema volume of rat of control group, at time t, and V_t is the edema volume of rat of test compound, at time t.

3 | RESULTS AND DISCUSSION

All the synthesized compounds are air stable and soluble in chloroform, DCM, DMF and DMSO. Analytical data of all the compounds are in good agreement with their proposed molecular formulae. Molecular structures of complexes were finally corroborated by single crystal X-ray diffraction studies. Analytical and spectral parameters are presented in Section 2.

3.1 | Spectral characterization

The numbering scheme of **LH$_3$** is given in Scheme 1. The IR spectrum of the **LH$_3$** (Figure S1) displayed characteristic absorption bands at 3444, 3326, 3232, 1680, 1660 and 1607 cm^{-1} due to ν (O-H), ν (N1-H), ν (N2-H), ν (C7 = O1), ν (C14 = O2) and ν (C=N), respectively. The band due to ν(C7 = O1) has remained almost unchanged in the spectra of all the complexes, suggesting its non-involvement in coordination. The band attributed to ν (C=N) in **LH$_3$** has shifted towards lower frequency upon complexation, indicating the involvement of azomethine nitrogen in coordination. The absence of bands due to ν (N2-H) and ν (C14 = O2) and the appearance of two new bands in the spectra of complexes at about 1611–1613 cm^{-1} and 1318–1324 cm^{-1} due to the stretching vibrations of the conjugated -C=N-N=C- and enolic C14-O2, respectively, indicate the enolization and subsequent coordination of oxygen atom to the central metal ion. In addition, the bands due to ν (C43 = O5)$_{amido}$ (in the amido form of ligand) and the one due to the new bond -C=N-N=C- (in the imidol form of ligand) in complex **4** are appearing at the same frequency (1612 cm^{-1}; Figure S2). The IR spectra of isomorphous complexes **5** (Figure S3) and **6** (Figure S4) are nearly identical with minor differences in the lower frequency region. The band observed in the region of 3420–3560 cm^{-1} in all complexes was assigned to ν (OH) of coordinated/lattice held water molecules. The *tert*-butyl substituent groups in **LH$_3$** and its complexes show their characteristic absorption patterns between 2866 and 2957 cm^{-1}.

The ^{1}H NMR spectrum of the **LH$_3$** (Figure S5) has shown three singlets at 12.33, 12.16 and 11.13 ppm due to the N2H, N1H and O3H, respectively. But the ^{1}H NMR spectrum of Ni(II) complex (**5**) (Figure S6) did not show any signals corresponding to either N2H or O3H, indicating the transformation of the ligand into the imidol form and further deprotonation prior to coordination with the metal ion. In addition, the ligand showed a sharp singlet due to an azomethine proton (C15-H) at 8.52 ppm. This signal is being shifted to 8.69 ppm due to the participation of azomethine nitrogen in coordination. The two sharp singlets in **LH$_3$**/**5** at 1.28/0.90 and 1.39/1.21 ppm correspond to two sets of magnetically non-equivalent *tert*-butyl groups.[32] The signals corresponding to the protons of aromatic moieties of **LH$_3$** and **5** were observed in the range of 7.2–8.25 and 6.73–8.18 ppm, respectively.

The ^{13}C NMR spectrum of **LH$_3$** (Figure S7) has showed signals at 164.32, 164.19 ppm and 155.18 ppm, assigned to carbonyl (C7 and C14) and azomethine (C15) carbons, respectively. The C14 and azomethine (C15) carbons exhibited downfield shifts in the Ni(II) complex (Figure S8). This suggests the involvement of enolic oxygen and azomethine nitrogen in the complexation. The two distinct resonances due to methyl carbons (−(CH$_3$)$_3$) of two non-equivalent *tert*-butyl groups in **LH$_3$**/**5** occurred at 29.77/29.8 and 31.74/30.79 ppm.

The ESI-MS of **LH$_3$** (Figure S9) shows a molecular ion peak [**LH$_3$** + H]$^+$ at 540. In the positive mode ESI-MS of **4**, the base peak observed at 1135 corresponds to mass of [(Co(**LH**)(**LH$_2$**)) + H]$^+$. This assignment is in good agreement with the ascribed +3 oxidation state for cobalt. ESI-MS analysis of **5** and **6** was done in DMSO with 0.1% NH$_4$OH solution. The aqua ligand present in both the complexes was replaced by NH$_3$. Hence, the peaks at 613 and 618 in the ESI-MS of **5** and **6** are assigned to [Ni(**LH**)(NH$_3$) + H]$^+$ and [Cu(**LH**)(NH$_3$) + H]$^+$, respectively. In addition, the intense peaks at 674 and 679 in **5** and **6** correspond to the DMSO adducts, i.e. [Ni(**LH**)(DMSO) + H]$^+$ and [Cu(**LH**)(DMSO) + H]$^+$, respectively.[33] The ESI and simulated mass spectra of all the complexes are provided as supplementary information (Figures S10a–S12c).

The UV–Vis absorption spectra of **LH$_3$** and its metal complexes were recorded in DMF solution and are displayed in Figure S13. **LH$_3$** displays two bands at 266 and 299 nm in the UV region, attributing to $\pi \rightarrow \pi^*$ and $n \rightarrow \pi^*$ transitions, respectively. After coordination with the metal ions, the $n \rightarrow \pi^*$ transition associated with azomethine chromophore is bathochromically shifted, indicating the involvement of imine nitrogen in coordination.[34] No d-d transitions could be observed in the case of **4** and **5**. The intense band that appeared at about 416–442 nm for the complexes has been assigned to charge transfer transitions. In the electronic spectrum of **6**, the broad band with peak maxima at 666 nm corresponds to the combination of $^2B_{1g} \rightarrow {}^2A_{1g}$ and $^2B_{1g} \rightarrow {}^2E_g$ transitions as expected for square-planar geometry.[35]

X-band EPR spectra were recorded in powder form as well as in frozen solution of [Cu(**LH**)(H$_2$O)]·H$_2$O (**6**) in methanol. The EPR signals of polycrystalline samples exhibit isotropic intense broad signals with $g_{iso} = 2.057$ with no hyperfine splitting (Figure S14). From solution EPR measurements, it was possible to resolve the hyperfine pattern (Figure S15) with $g_{\parallel} = 2.245$, $g_{\perp} = 2.034$, $g_{av} = 2.104$, G = 7.206, $A_{\parallel} = 154 \times 10^{-4}$ cm^{-1} and $A_{\perp} = 34 \times 10^{-4}$ cm^{-1}. The spectrum shows typical axial behavior with tensor values of $g_{\parallel} > g_{\perp} > g_e$ (2.0023), which are consistent with a $d_{x^2-y^2}$ ground state.[36] The axial symmetry parameter, G, quantifies the exchange interaction between copper centers in a polycrystalline compound. It is calculated by using the equation $G = g_{\parallel} - 2/g_{\perp} - 2$. As G > 4, it is expected that there is no exchange coupling between two copper centers.[37] The empirical factor $f = g_{\parallel}/A_{\parallel}$ measures the degree of tetrahedral distortion.

The f value for complex **6** is 146 indicating a small distortion from planarity.[38] According to Kivelson and Neiman,[39] the ground state molecular orbital coefficient, α^2, can be taken as a measure of metal–ligand covalency and is calculated by the following equation

$$\alpha^2 = \frac{-A_{\parallel}}{0.036} + \left(g_{\parallel} - 2.0023\right) + \frac{3}{7}(g_{\perp} - 2.0023) + 0.04$$

The above-calculated value for α^2 (0.72) for **6** is evidence for the partial covalent character of the complex.

3.2 | Thermal analysis

The TG and DT analyses of the crystalline complexes were carried out in the temperature range of 25–1000°C under a nitrogen atmosphere. Complex **4** is stable up to 170°C. It undergoes thermal decomposition in three steps (Figure S16). The first step occurring at 170–200°C corresponds to the liberation of hydrogen bonded enclathrated water molecule (found 1.62%, calcd 1.57%). The second step decomposition appears in the range 200–350°C, indicating the decomposition of part of the ligand. The last step observed in the range 350–580°C corresponds to the decomposition of the remaining part of the ligand. The plateau obtained above 580°C corresponds to the formation of stable cobalt oxide with the residual weight of 7.34%. The TG/DTA curves of **5** (Figure S17) show the first exothermic weight loss (found 2.91%, calcd 2.85%) at 70°C, and is consistent with the removal of hydrogen bonded enclathrated water molecule. In the second stage, coordinated aqua ligand (found 2.93%, calcd 2.85%) is lost in the range 85–120°C with an exothermic DTA curve at 105°C. The third and fourth step observed in the temperature range 120–510°C involve the removal of organic component. The residual weight of 12% above 510°C corresponds to NiO. The TG and DT data of **6** are similar to **5** and are in good agreement with the crystallographic structure.

3.3 | Single crystal X-ray diffraction studies

The crystallographic data of all three complexes are summarized in Table 1. The molecular structures of **4**, **5** and **6** along with atom numbering schemes are portrayed in Figures 1–3, respectively. Table 2 lists selected bond lengths and bond angles. Relevant hydrogen bond interactions are compiled in Table S1.

3.3.1 | Structural descriptions of [Co(LH)(LH_2)]·H_2O (4)

The crystallographic asymmetric unit of complex **4** comprises two independent molecules of [Co(**LH**)(**LH_2**)] (**4A** and **4B**) and two lattice held water of crystallization. These two molecules (**4A** and **4B)** are crystallographically non-equivalent and chemically equivalent. The compound crystallizes in orthorhombic system with $P2_12_12_1$ space group, and the Co(III) center exhibits a distorted octahedral coordination where two inequivalent *ONO* tridentate ligands [that differ in their protonation state (**LH^{2-}** and **LH_2^-**); Scheme 2], coordinate metal ions through phenolic oxygen atoms [(O3a, O5a) in **4A**; (O3b, O5b) in **4B**], imine nitrogens [(N3a, N6a) in **4A**; (N3b, N6b) in **4B**], enolic oxygens [O2a in **4A**; O2b in **4B**] and carbonyl oxygens [O5a in **4A**; O5b in **4B**]. In both the molecules, the chloro atom present in the ortho position of the 2,4-dichlorophenyl group (in **LH_2^-**) exhibits twofold rotational disorder (Figure S18). The chlorine atoms Cl3a (in **4A**) and Cl3b (in **4B**) have major occupancy of 0.879(4) and 0.844(5), respectively. In the coordination sphere, both the ligands (**LH^{2-}** and **LH_2^-)** in molecule **4A** and molecule **4B** are almost perpendicular to each other. Azomethine nitrogens [(N3a and N6a) in **4A**; (N3b and N6b) in **4B**] of the two ligands reside *trans* to each other, whereas the other two donor sites [(O2a, O5a) and (O3a, O6a) in **4A**; (O2b, O5b) and (O3b, O6b) in **4B**] have remained *cis* to each other, i.e. the ligands coordinate to the metal in a meridional fashion. The coexistence of both the tautomeric forms of ligand within a complex is substantiated by the bond distances in the region of five-membered chelate rings (Co1A/N3A/N2A/C14A/O2A and Co1A/N6A/N5A/C43A/O5A in **4A** and Co1B/N3B/N2B/C14B/O2B and Co1B/N6B/N5B/C43B/O5B in **4B**). The C14-$O2_{imidol}$ [1.311(5) Å in **4A**, 1.312(5) Å in **4B**] and C43-$O5_{amido}$ [1.275(5) Å in **4A**, 1.264(5) Å in **4B**] differ in their lengths. The N5-C43 [1.333(5) Å in **4A**, 1.332(5) Å in **4B**] is more of σ in character compared with N2-C14 [1.304(6) Å in **4A**, 1.298(6) Å in **4B**]. The bite angles for the ligands (**LH^{2-}** and **LH_2^-**) lie in the range 82.52–96.38°, indicating a distortion from an ideal octahedral geometry, with the *trans*-donor bond angles in the range 173.71–176.94° (in **4A**); 175.33–177.73° (in **4B**) and the *cis*-donor bond angles in the range 82.52–95.92° (in **4A**); 83.29–96.38° (in **4B**).

The enclathrated water molecules donate hydrogen bonds to enolic and carbonyl oxygen atoms, and receive hydrogen bonds from the amide nitrogen atom (Figure S19). In addition, the molecular structure is stabilized by various C-H···π interactions (Figure S20).

TABLE 1 Crystal data and structure refinement details of the complexes **4**, **5** and **6**

Compound code	4	5	6
Empirical formula	$C_{58}H_{61}Cl_4CoN_6O_7$	$C_{29}H_{33}Cl_2N_3NiO_5$	$C_{29}H_{33}Cl_2CuN_3O_5$
Formula weight	1154.85	633.19	638.02
Temperature/K	100(1)	100(1)	100(1)
Wavelength/Å	1.54184	1.54184	1.54184
Crystal system	orthorhombic	monoclinic	monoclinic
Space group	$P2_12_12_1$	$P2_1/c$	$P2_1/c$
Unit cell dimensions			
a/Å	14.8111(2)	12.48634(14)	12.35369(16)
b/Å	23.7501(4)	18.5110(2)	18.5750(3)
c/Å	32.2876(5)	12.93851(19)	13.08052(19)
α/°	90	90	90
β/°	90	103.2443(13)	104.1404(14)
γ/°	90	90	90
Volume/Å^3	11 357.6(3)	2910.99(6)	2910.63(7)
Z	8	4	4
Density (calculated) g cm^{-3}	1.351	1.445	1.456
Absorption coefficient/mm^{-1}	4.563	3.010	3.108
F(000)	4816.0	1320.0	1324.0
Crystal size/mm^3	0.170 × 0.130 × 0.080	0.337 × 0.305 × 0.182	0.170 × 0.120 × 0.100
2 theta range for data collection/°	5.474 to 149	7.272 to 148.934	7.38 to 148.962
Index ranges	$-18 \le h \le 17$, $-22 \le k \le 29$, $-40 \le l \le 39$	$-13 \le h \le 15$, $-23 \le k \le 22$, $-16 \le l \le 13$	$-15 \le h \le 14$, $-23 \le k \le 23$, $-16 \le l \le 16$
Reflections collected	33 685	13 472	12 953
Independent reflections	20 461 [R_{int} = 0.0318, R_{sigma} = 0.0496]	5937 [R_{int} = 0.0205, R_{sigma} = 0.0254]	5942 [R_{int} = 0.0175, R_{sigma} = 0.0244]
Absorption correction Semi-empirical from equivalents	Multi-scan	Gaussian	Multi-scan
Data/restraints/parameters	20 461/2/1454	5937/0/387	5942/0/387
Goodness-of-fit on F^2	1.044	1.042	1.003
Final R indexes [$I \ge 2\sigma(I)$]	R_1 = 0.0468, wR_2 = 0.1115	R_1 = 0.0307, wR_2 = 0.0801	R_1 = 0.0288, wR_2 = 0.0748
Final R indexes [all data]	R_1 = 0.0581, wR_2 = 0.1194	R_1 = 0.0329, wR_2 = 0.0816	R_1 = 0.0331, wR_2 = 0.0781
Largest diff. peak and hole/e Å^{-3}	0.78/−0.50	0.28/−0.45	0.33/−0.43

3.3.2 | Structural descriptions of [Ni(LH)(H$_2$O)]·H$_2$O (5) and [Cu(LH)(H$_2$O)]·H$_2$O (6)

Complexes **5** and **6** are isomorphous structures where different divalent cations are present [Ni(II) in **5** and Cu(II) in **6**]. Both complexes crystallize in the monoclinic system with $P2_1/c$ space group and each asymmetric unit contains neutral [M(L)(H$_2$O)] (M = Ni, **5**; Cu, **6**) along with one lattice held water of crystallization. The Ni(II) or Cu(II) centers display a slightly tetrahedrally distorted square-planar coordination provided by two oxygen (O2, O3) and one nitrogen (N3) atoms of the doubly deprotonated *ONO* tridentate hydrazone (**LH^{2-}**) and one oxygen atom (O4) of aqua ligand. The C14-O2 bond length [1.311(17) Å in **5**, 1.305 (19) Å in **6**] is of single-bond character, and C14-N2 [1.311(19) Å in **5**, 1.317 (2) Å in **6**] is of double-bond character, this indicates the enolization and subsequent coordination of oxygen atom

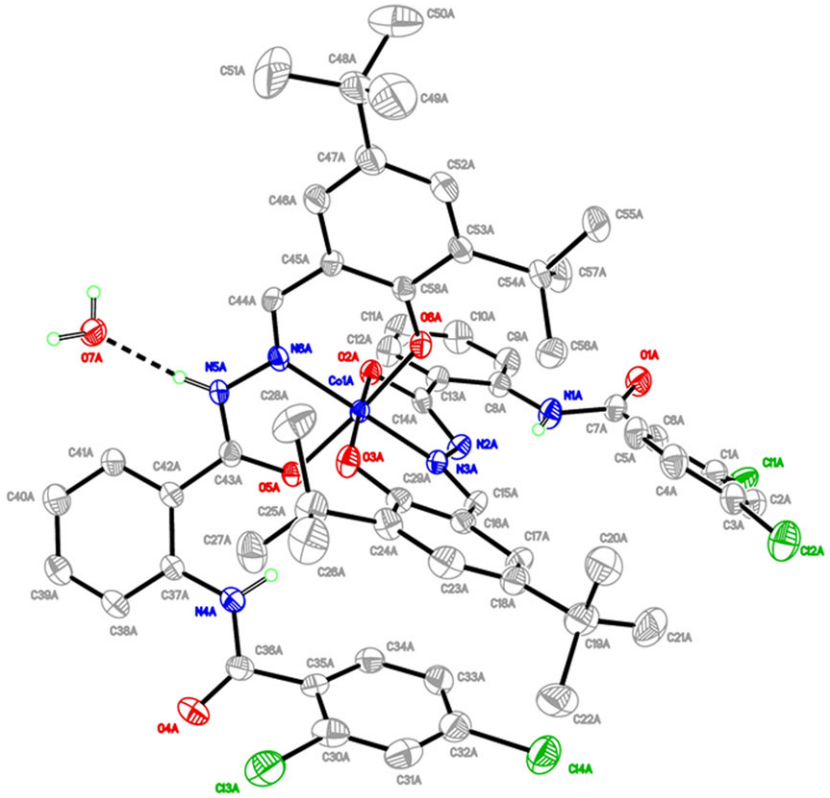

FIGURE 1 ORTEP projection of **4A** (drawn at 50% probability level) with partial atom-numbering scheme. Disordered atoms and H-atoms attached to carbon omitted for clarity

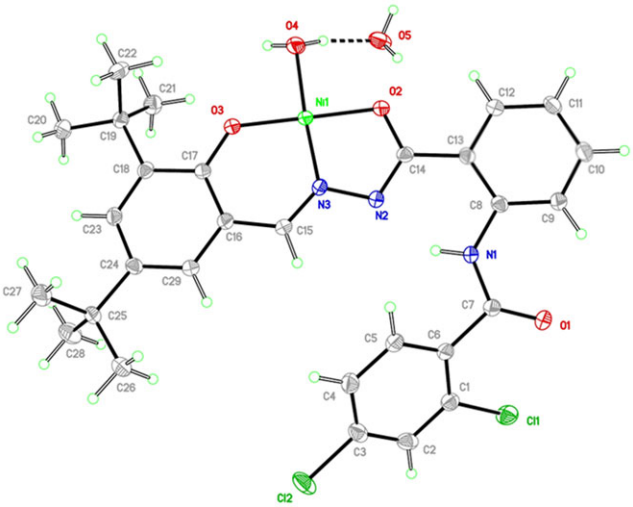

FIGURE 2 ORTEP projection of **5** showing 50% probability ellipsoids

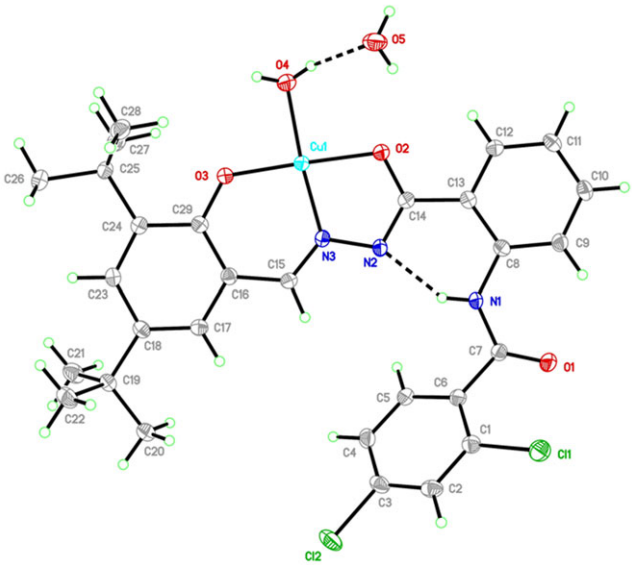

FIGURE 3 ORTEP projection of **6** showing 50% probability ellipsoids

(O2) to the central metal ion via deprotonation. The ligand has formed one five- and one six-membered chelate ring with the metal center. The bite angles O2-M-N3 (84.62° in **5**; 82.51° in **6**) and N3-M-O3 (96.51° in **5**; 95.94° in **6**) indicate significant deviation from ideal square-planar geometry in the complexes.[40] The M-O bond lengths in **5** and **6** are in the range of 1.809–1.921 Å and 1.860–1.974 Å, respectively. The M-N bond lengths in **5** and **6** are 1.798(12) Å and 1.885(12) Å, respectively. These bond lengths are close to the reported analogous square-planar Ni(II) and Cu(II) complexes.[41,42]

TABLE 2 Selected bond lengths (Å) and angles (^{0}) of the complexes **4**, **5** and **6**

4			
Molecule 4A		**Molecule 4B**	
Co1A-O3A	1.859(3)	Co1B-O3B	1.851(3)
Co1A-N3A	1.864(4)	Co1B-N3B	1.867(4)
Co1A-O6A	1.869(3)	Co1B-O6B	1.881(3)
Co1A-N6A	1.890(4)	Co1B-N6B	1.893(4)
Co1A-O2A	1.930(3)	Co1B-O2B	1.923(3)
Co1A-O5A	1.955(3)	Co1B-O5B	1.962(3)
O2A-C14A	1.311(5)	O2B-C14B	1.312(5)
O3A-C29A	1.327(5)	O3B-C29B	1.319(6)
O5-C43A	1.275(5)	O5B-C43B	1.264(5)
O6A-C58A	1.313(5)	O6B-C58B	1.316(5)
N2A-C14A	1.304(6)	N2B-C14B	1.298(6)
N2A-N3A	1.395(5)	N2B-N3B	1.399(5)
N3A-C15A	1.286(5)	N3B-C15B	1.283(6)
N5A-C43A	1.333(6)	N5B-C43B	1.332(6)
N5A-N6A	1.379(5)	N5B-N6B	1.391(5)
N6A-C44A	1.296(6)	N6B-C44B	1.281(6)
O3A-Co1A-N3A	93.41(15)	O3B-Co1B-N3B	94.15(15)
O3A-Co1A-O6A	93.11(15)	O3B-Co1B-O6B	92.82(15)
N3A-Co1A-O6A	88.18(14)	N3B-Co1B-O6B	87.92(15)
O3A-Co1A-N6A	89.15(15)	O3B-Co1B-N6B	87.83(15)
N3A-Co1A-N6A	176.94(16)	N3B-Co1B-N6B	177.73(16)
O6A-Co1A-N6A	93.36(15)	O6B-Co1B-N6B	93.10(15)
O3A-Co1A-O2A	173.71(15)	O3B-Co1B-O2B	175.33(15)
N3A-Co1A-O2A	82.92(14)	N3B-Co1B-O2B	83.29(14)
O6A-Co1A-O2A	91.87(14)	O6B-Co1B-O2B	91.00(14)
N6A-Co1A-O2A	94.38(15)	N6B-Co1B-O2B	94.65(14)
O3A-Co1A-O5A	87.24(14)	O3B-Co1B-O5B	87.62(14)
N3A-Co1A-O5A	95.92(14)	N3B-Co1B-O5B	96.38(14)
O6A-Co1A-O5A	175.86(13)	O6B-Co1B-O5B	175.64(14)
N6A-Co1A-O5A	82.52(14)	N6B-Co1B-O5B	82.58(14)
O2A-Co1A-O5A	88.07(13)	O2B-Co1B-O5B	88.78(14)
5		**6**	
Ni1-N3	1.7978(12)	Cu1-N3	1.8850(13)
Ni1-O2	1.8597(10)	Cu1-O2	1.9334(11)
Ni1-O3	1.8090(10)	Cu1-O3	1.8604(11)
Ni1-O4	1.9208(12)	Cu1-O4	1.9738(13)
O2-C14	1.3111(17)	O2-C14	1.3054(19)
O3-C17	1.3196(17)	O3-C29	1.3170(19)
N2-C14	1.3107(19)	N2-C14	1.317(2)

(Continues)

TABLE 2 (Continued)

4			
Molecule 4A		**Molecule 4B**	
N2-N3	1.3957(16)	N2-N3	1.3956(18)
N3-C15	1.3004(19)	N3-C15	1.296(2)
N3-Ni1-O3	96.51(5)	O3-Cu1-N3	95.44(5)
N3-Ni1-O2	84.62(5)	O3-Cu1-O2	176.43(5)
O3-Ni1-O2	177.99(5)	N3-Cu1-O2	82.51(5)
N3-Ni1-O4	175.94(5)	O3-Cu1-O4	89.23(5)
O3-Ni1-O4	87.26(5)	N3-Cu1-O4	174.83(6)
O2-Ni1-O4	91.56(5)	O2-Cu1-O4	92.71(5)

The molecular structures of **5** and **6** are stabilized by intra-molecular hydrogen bond interactions, N1-H1A···N2. In both **5** and **6**, enclathrated water molecule is involved in three different hydrogen interactions (Figures S21 and S22). O5 of lattice water acts as hydrogen bond donor to the carbonyl oxygen (O1) and deprotonated imido oxygen (O2) of two adjacent molecules, and also as hydrogen bond acceptor from oxygen (O4) of aqua ligand. In the case of **5** and **6**, only one of the two available O-H bonds of aqua ligand is utilized in the hydrogen bonding, thereby breaking Etter's first rule of hydrogen bonding.[43] The structures of **5** and **6** are additionally stabilized by various intermolecular π···π interactions. The π···π interactions present in **5** and **6** are depicted in Figures S23 and S24, respectively. No significant C-H···π interactions are observed.

3.4 | Biological studies

The stability of the metal complexes (**4–6**) in DMF and DMSO was checked by comparing the UV–Vis spectra of the complexes over a period of 5 h (Figure S25). No significant change was observed, which indicates that the complexes are stable in DMF and DMSO for the first 5 h.

3.4.1 | Antioxidant activity

In vitro antioxidant activity of the newly synthesized hydrazone (**LH_3**) and its complexes was evaluated using the DPPH free radical scavenging assay. In the present investigation, **LH_3** and its metal complexes have shown a dose-dependent response (Figure S26). The DPPH scavenging activity of all compounds is expressed as the IC_{50} values. The IC_{50} values of **LH_3**, **4**, **5** and **6** complexes are 85.76, 42.36, 78.54 and 57.54 ppm, respectively (Table 3). Comparison of the activity exhibited by **LH_3** and its complexes indicates that the metal complexes exhibit better activity than the ligands themselves due to their enhanced lipophilicities. Among the complexes, the Co(III) complex exhibited significant DPPH radical scavenging activity. Compared with ascorbic acid taken as a standard drug, the activity shown by reported compounds is less.

3.4.2 | Anti-inflammatory activity

The *in vivo* anti-inflammatory activity of the metal complexes along with parent ligand was evaluated by the functional model of carrageenan-induced rat paw edema. There are biphasic effects in carrageenan-induced edema.[44,45] The early phase is mainly mediated by histamine, 5-HT, serotonin and kinins[46], whereas the latter phase is protracted by the release of prostaglandins and leukotriens derived from arachidonic acid[7], thus the feet rapidly became swollen, reaching close to the control's level by 3 h. The experimental results (Figure S27; Table 4) exhibit the effective inhibitory activity of the synthesized compounds on both phases of carrageenan-induced paw inflammation. All the compounds have shown suppression of edema in a dose-dependent manner. Compared with **LH_3**, its metal complexes have exhibited better activity, and this may be due to chelation, which reduces the polarity of the central metal ion because of partial sharing of its positive charge with the donor atoms of the ligand, thus increasing the lipophilic nature of the metal.[47,48] Compared with diclofenac taken as a standard drug, the activity shown by reported compounds is less. **LH_3** is active at 10 mg kg^{-1} dose with a percentage inhibition of 85.41%. Among all complexes, **6** has shown promising activity

TABLE 3 DPPH radical scavenging activity of LH_3 and its metal complexes

Samples	% Radical scavenging activity at different concentrations ($\mu g\ ml^{-1}$)					IC_{50} ($\mu g\ ml^{-1}$)
	20	40	60	80	100	
LH_3	13.59 ± 1.74	22.23 ± 3.62	32.69 ± 2.66	40.86 ± 1.39	58.30 ± 1.75	85.76
4	33.20 ± 1.74	47.21 ± 1.81	66.22 ± 1.31	77.90 ± 1.99	88.30 ± 1.12	42.36
5	20.00 ± 1.74	27.88 ± 2.20	38.19 ± 1.59	50.93 ± 1.09	63.85 ± 1.25	78.54
6	24.58 ± 0.96	35.60 ± 1.16	52.14 ± 1.63	66.10 ± 1.99	76.44 ± 2.61	57.54
Ascorbic acid	39.60 ± 1.21	55.72 ± .93	74.18 ± 1.71	82.58 ± 1.07	93.12 ± 2.60	35.89

Results expressed in mean ± SEM ($n = 3$). ANOVA followed by Tukey's multiple comparison test.

TABLE 4 Anti-inflammatory activity of LH_3 and its metal complexes

Groups	Paw volume in ml (% of edema inhibition)			
	0.5 h	1 h	3 h	5 h
Control	1.097 ± 0.044	1.197 ± 0.014	1.170 ± 0.062	1.343 ± 0.028
Diclofenac (10 mg kg^{-1})	0.030 ± 0.027*** (97.26%)	0.030 ± 0.027*** (97.49%)	0.108 ± 0.040*** (90.77%)	0.025 ± 0.013*** (98.14%)
LH_3 (5 mg kg^{-1})	0.383 ± 0.082*** (65.08%)	0.480 ± 0.098*** (59.90%)	0.687 ± 0.138*** (41.28%)	0.483 ± 0.080*** (64.03%)
LH_3 (10 mg kg^{-1})	0.160 ± 0.086*** (85.41%)	0.370 ± 0.109*** (69.08%)	0.653 ± 0.098*** (44.18%)	0.330 ± 0.080*** (75.43%)
4 (5 mg kg^{-1})	0.421 ± 0.034*** (62.62%)	0.316 ± 0.053*** (73.60%)	0.578 ± 0.055*** (60.60%)	0.324 ± 0.024*** (75.87%)
4 (10 mg kg^{-1})	0.331 ± 0.074*** (69.82%)	0.247 ± 0.032*** (79.36%)	0.833 ± 0.045*** (28.80%)	0.203 ± 0.004*** (84.88%)
5 (5 mg kg^{-1})	0.256 ± 0.038*** (76.66%)	0.196 ± 0.026*** (83.62%)	0.960 ± 0.048 (17.95%)	0.243 ± 0.009*** (81.90%)
5 (10 mg kg^{-1})	0.183 ± 0.042*** (83.31%)	0.130 ± 0.043*** (89.14%)	0.790 ± 0.041** (32.48%)	0.217 ± 0.061*** (83.84%)
6 (5 mg kg^{-1})	0.276 ± 0.055*** (74.84%)	0.250 ± 0.032*** (79.11%)	0.917 ± 0.090 (21.62%)	0.210 ± 0.017*** (84.36%)
6 (10 mg kg^{-1})	0.103 ± 0.024*** (90.61%)	0.230 ± 0.064*** (80.78%)	0.887 ± 0.033 (24.19%)	0.194 ± 0.044*** (85.55%)

Results expressed in mean ± SEM ($n = 6$). ANOVA followed by Dunnett's test.

**$P < 0.01$. ***$P < 0.001$ when compared with control group.

with a percentage inhibition of 90.61% in the early phase of inflammation (0.5 h). Anti-inflammatory activity of the synthesized metal complexes is greater compared with corresponding metal salts (Table S2).

4 | CONCLUSION

Mononuclear Co(III), Ni(II) and Cu(II) complexes of 2-(2,4-dichlorobenzamido)-*N′*-(3,5-di-*tert*-butyl-2-hydroxybenzylidene)benzohydrazide were synthesized and structurally characterized by X-ray crystallography. The molecular structure of complex **4** divulges that both the tautomeric forms of ligand are associated with the Co (III) ion in a meridonial fashion, and adopts a distorted octahedral geometry. While in isomorphous complexes **5** and **6**, ligand coordinated to central metal through imidol tautomeric form, and results into distorted square-planar geometry. The anti-inflammatory and antioxidant activities of the three complexes and the ligand were evaluated simultaneously. We found that all the compounds showed considerable activity in a concentration-dependent manner. Among the compounds tested, metal complexes have shown higher activity than parent ligands perhaps due to their enhanced lipophilicities.

ACKNOWLEDGEMENTS

The authors thank USIC, Karnatak University, Dharwad, Sophisticated Analytical Instrument Facility-CDRI Lucknow and Indian Institute of Science, Bangalore for spectral analyses. The authors sincerely thank Mr Shreekanth Aili for his help in carrying out *in vivo* anti-inflammatory activity. One of the authors (G. H. Chimmalagi) is grateful to UGC, for awarding RFSMS fellowship.

ORCID

Kalagouda B. Gudasi http://orcid.org/0000-0002-0063-7656

REFERENCES

[1] T. Mittag, *Exp. Eye Res.* **1984**, *39*, 759.

[2] S. P. Wolff, A. Garner, R. T. Dean, *Trends Biochem. Sci.* **1986**, *11*, 27.

[3] R. M. Abolfath, A. C. T. van Duin, T. Brabec, J. Phys, *Chem. A* **2011**, *115*, 11 045.

[4] D. Dreher, A. F. Junod, *Eur. J. Cancer* **1996**, *32A*, 30.

[5] B. Uttara, A. V. Singh, P. Zamboni, R. T. Mahajan, *Curr. Neuropharmacol.* **2009**, *7*, 65.

[6] K. Sugamura, J. F. Keaney Jr., *Free Radic. Biol. Med.* **2011**, *51*, 978.

[7] N. K. Boughton-Smith, A. M. Deakin, R. L. Follenfant, B. J. R. Whittle, L. G. Garland, *Br. J. Pharmacol.* **1993**, *110*, 896.

[8] T. Sumiya, Y. Fujimoto, H. Nishida, Y. Morikawa, S. Sakuma, T. Fujita, *Free Radic. Biol. Med.* **1993**, *15*, 101.

[9] J. Martel-Pelletier, D. Lajeunesse, P. Reboul, *Ann. Rheum. Dis.* **2003**, *62*, 501.

[10] A. Tadić, J. Poljarević, M. Krstić, M. Kajzerberger, S. Aranđelović, S. Radulović, C. Kakoulidou, A. N. Papadopoulos, G. Psomas, S. Grgurić-Šipkaa, *New J. Chem.* **2018**, *42*, 3001. https://doi.org/10.1039/C7NJ04416J

[11] M. Zampakou, N. Rizeq, V. Tangoulis, A. N. Papadopoulos, F. Perdih, I. Turel, G. Psomas, *Inorg. Chem.* **2014**, *53*, 2040.

[12] A. Stadler, J. Harrowfield, *Inorg. Chim. Acta* **2009**, *362*, 4298.

[13] D. S. Badiger, R. B. Nidavani, R. S. Hunoor, B. R. Patil, R. S. Vadavi, V. M. Chandrashekhar, I. S. Muchchandi, K. B. Gudasi, *Appl. Organomet. Chem.* **2011**, *25*, 876.

[14] S. A. Aboafia, S. A. Elsayed, A. K. A. El-Sayed, A. M. El-Hendawy, *J. Mol. Struct.* **2018**, *1158*, 39.

[15] Y. Du, W. Chen, X. Fu, H. Deng, J. Deng, *RSC Adv.* **2016**, *6*. 109 718

[16] M. Sutradhar, L. M. D. R. S. Martins, M. Fátima, C. Guedes da Silva, K. T. Mahmudov, C. Liu, A. J. L. Pombeiro, *Eur. J. Inorg. Chem.* **2015**, *2015*, 3959.

[17] M. Sutradhar, E. C. B. A. Alegria, T. R. Barman, F. Scorcelletti, M. Fátima, C. Guedes da Silva, A. J. L. Pombeiro, *Mol. Catal.* **2017**, *439*, 224.

[18] S. Misra, S. Ghatak, N. Patil, P. Dandawate, V. Ambike, S. Adsule, D. Unni, K. Venkateswara Swamy, S. Padhye, *Bioorg. Med. Chem.* **2013**, *21*, 2551.

[19] S. M. Patil, R. S. Vadavi, S. Dodamani, U. Kendur, G. Chimmalagi, S. Jalalpure, C. S. Frampton, K. B. Gudasi, *Transition Met. Chem.* **2018**, *43*, 65.

[20] S. Ghatak, A. Vyas, S. Misra, P. O'Brien, A. Zambre, V. M. Fresco, R. R. Markwald, K. Venkateshwara Swamy, Z. Afrasiabi, A. Choudhury, M. Khetmalas, S. Padhye, *Bioorg. Med. Chem. Lett.* **2014**, *24*, 317.

[21] M. Sutradhar, E. C. B. A. Alegria, K. T. Mahmudov, M. F. C. Guedes da Silva, A. J. L. Pombeiro, *RSC Adv.* **2016**, *6*, 8079.

[22] M. Sutradhar, M. V. Kirillova, M. Fátima, C. Guedes da Silva, C. Liuc, A. J. L. Pombeiro, *Dalton Trans.* **2013**, *42*. 16 578.

[23] D. Matoga, J. Szklarzewicz, K. Stadnicka, M. S. Shongwe, *Inorg. Chem.* **2007**, *46*, 9042.

[24] X. Peng, X. Tang, W. Qin, W. Dou, Y. Guo, J. Zheng, W. Liu, D. Wang, *Dalton Trans.* **2011**, *40*, 5271.

[25] A. I. Vogel, *A Textbook of Quantitative Inorganic Analysis*, 3rd ed., Longmans Green, London **1961**.

[26] G. H. Chimmalagi, U. Kendur, S. M. Patil, K. B. Gudasi, C. S. Frampton, M. B. Budri, C. V. Mangannavar, I. S. Muchchandi, *Appl. Organomet. Chem.* **2018**, *32*. https://doi.org/10.1002/aoc.4337

[27] CrysAlis*PRO* Software system, *Version 1.171.38.41, Rigaku Oxford Diffraction*, Rigaku, Oxford, UK **2015**.

[28] G. Sheldrick, *Acta Crystallogr. C* **2015**, *71*, 3.

[29] C. F. Macrae, I. J. Bruno, J. A. Chisholm, P. R. Edgington, P. McCabe, E. Pidcock, L. Rodriguez-Monge, R. Taylor, J. van de Streek, P. A. Wood, *J. Appl. Cryst.* **2008**, *41*, 466.

[30] R. P. Singh, K. N. C. Murthy, G. K. Jayaprakasha, *J. Agric. Food Chem.* **2002**, *50*, 81.

[31] C. A. Winter, E. A. Risley, G. W. Nuss, *Exp. Biol. Med.* **1962**, *111*, 544.

[32] J. Figuerasp, P. W. Scullardan, A. R. Mack, *J. Org. Chem.* **1971**, *36*, 3497.

[33] S. J. Fischer, L. M. Benson, A. Fauq, S. Naylor, A. J. Windebank, *Neurotoxicology* **2008**, *29*, 444.

[34] J. R. Anacona, V. Rangel, M. Lorono, J. Camus, *Spectrochim. Acta Mol.* **2015**, *149*, 23.

[35] I. Casanova, A. Sousa-Pedrares, J. Viqueira, M. L. Durán, J. Romero, A. Sousa, J. A. García-Vázquez, *New J. Chem.* **2013**, *37*, 2303.

[36] S. Chandra, K. B. Pandeya, R. P. Singh, *Indian J. Chem.* **1979**, *18A*, 476.

[37] B. J. Hathaway, D. E. Billing, *Coord. Chem. Rev.* **1970**, *5*, 143.

[38] U. Sakaguchi, A. W. Addison, *J. Chem. Soc. Dalton Trans.* **1979**, *4*, 600.

[39] D. Kivelson, R. Neiman, *J. Chem. Phys.* **1961**, *35*, 149.

[40] S. Saha, S. Jana, S. Gupta, A. Ghosh, H. P. Nayek, *Polyhedron* **2016**, *107*, 183.

[41] P. Sathyadevi, P. Krishnamoorthy, R. R. Butorac, A. H. Cowley, N. S. P. Bhuvanesh, N. Dharmaraj, *Dalton Trans.* **2011**, *40*, 9690.

[42] U. Kendur, G. H. Chimmalagi, S. M. Patil, K. B. Gudasi, C. S. Frampton, C. V. Mangannavar, I. S. Muchchandi, *J. Mol. Struct.* **2018**, *1153*, 299.

[43] M. C. Etter, *Acc. Chem. Res.* **1990**, *23*, 120.

[44] I. Posadas, M. Bucci, F. Roviezzo, A. Rossi, L. Parente, L. Sautebin, G. Cirino, *Br. J. Pharmacol.* **2004**, *142*, 331.

[45] R. Vinegar, W. Schreiber, R. Hugo, *J. Pharmacol. Exp. Ther.* **1969**, *166*, 96.

[46] M. Di Rosa, J. P. Giroud, D. A. Willouchby, *J. Pathol.* **1971**, *104*, 15.

[47] A. Jamadar, A. Duhme-Klair, K. Vemuri, M. Sritharan, P. Dandawatec, S. Padhye, *Dalton Trans.* **2012**, *41*, 9192.

[48] R. S. Hunoor, B. R. Patil, D. S. Badiger, R. S. Vadavi, K. B. Gudasi, V. M. Chandrashekhar, I. S. Muchchandi, *Appl. Organomet. Chem.* **2011**, *25*, 476.

SUPPORTING INFORMATION

Additional supporting information may be found online in the Supporting Information section at the end of the article.

How to cite this article: Chimmalagi GH, Kendur U, Patil SM, et al. Mononuclear Co(III), Ni(II) and Cu(II) complexes of 2-(2,4-dichlorobenzamido)-*N*′-(3,5-di-*tert*-butyl-2-hydroxybenzylidene)benzohydrazide: Structural insight and biological assay. *Appl Organometal Chem*. 2019;33:e4557. https://doi.org/10.1002/aoc.4557